Mapping the Functional Surface of Domain 2 in the Gelsolin Superfamily[†,‡]

Yoram A. Puius,[§] Elena V. Fedorov,[§] Ludwig Eichinger,[||] Michael Schleicher,[||] and Steven C. Almo*[,§]

Department of Biochemistry, Albert Einstein College of Medicine, 1300 Morris Park Avenue, Bronx, New York 10461, and Adolf-Butenandt-Institut/Zellbiologie, Ludwigs-Maximilians Universität München, Schillerstrasse 42, 80336 München, FRG

Received October 11, 1999; Revised Manuscript Received January 19, 2000

ABSTRACT: The crystal structure of the F-actin binding domain 2 of severin, the gelsolin homologue from *Dictyostelium discoideum*, has been determined by multiple isomorphous replacement and refined to 1.75 Å resolution. The structure reveals an α-helix−β-sheet sandwich similar to the domains of gelsolin and villin, and contains two cation-binding sites, as observed in other domain 1 and domain 2 homologues. Comparison of the structures of several gelsolin family domains has identified residues that may mediate F-actin binding in gelsolin domain 2 homologues. To assess the involvement of these residues in F-actin binding, three mutants of human gelsolin domain 2 were assayed for F-actin binding activity and thermodynamic stability. Two of the mutants, RRV168AAA and RLK210AAA, demonstrated a lowered affinity for F-actin, indicating a role for those residues in filament binding. Using both structural and biochemical data, we have constructed a model of the gelsolin domain 1−domain 2−F-actin complex. This model highlights a number of interactions that may serve as positive and negative determinants of filament end- and side-binding.

Gelsolin and its homologues are actin-regulatory proteins, composed of three to six repeats of an ancestral 15 kDa domain, whose sequences, structures, and functions are conserved from slime molds to humans (*1*−*3*). Family members are typically activated by calcium to bind to the side of an actin filament, sever the filament, and then cap its barbed end with picomolar affinity (*2*). Gelsolin can be dissociated from the barbed end by phosphoinositides such as PIP_2, which is thought to be the physiological mechanism of uncapping (*4*). Domain 1 binds the barbed ends of actin filaments (as well as monomeric actin, which serves as a barbed end mimic), while domain 2 binds exclusively to the sides of actin filaments. Gelsolin plays a role in remodeling the actin cytoskeleton during cell locomotion, and has been implicated in apoptosis, G-protein and phospholipase signaling, and tumor suppression (*5*−*7*).

The mechanism by which gelsolin binds, severs, and caps filaments is not completely understood, and an atomic model of the complex of F-actin and full-length gelsolin is not available. Although the interaction between gelsolin domain 1 and the barbed end of the filament has been described in the crystal structure of the gelsolin domain 1−G-actin complex (*8*), at present, the molecular interactions between gelsolin domain 2 and F-actin are not well-defined. McLaughlin et al. (*8*) had originally proposed that gelsolin domain 2 bound between the two strands of the filament, but more recent studies suggest that gelsolin domain 2 bound along the actin filament axis instead (*9*, *10*).

Residues in gelsolin domain 2 homologues which mediate side-binding activity have been suggested by studies demonstrating that peptides derived from gelsolin domain 2 (residues 198−227) (*11*, *12*) or villin domain 2 (residues 132−147, corresponding to gelsolin domain 2 residues 159−171) (*13*) display a weak affinity for F-actin. Consistent with these observations, deletion mapping has implicated residues 161−172 of gelsolin in F-actin binding (*14*). However, it is unclear whether these peptides and truncated proteins retain the conformation of the native protein. Additionally, studies of basic peptides with different sequences suggest that peptide−F-actin interactions may be nonspecific and electrostatic in nature, as seen in peptides derived from villin domain 2 (*13*) and from other F-actin binding proteins (*15*).

The most direct information describing the interactions between gelsolin domain 2 and F-actin are the helical reconstructions of actin filaments decorated with gelsolin domains 2 and 3 or domains 2−6 (*16*). These studies revealed that the gelsolin-binding site on F-actin involves subdomains 1 and 3 of the upper monomer and subdomains 1 and 2 of the lower monomer. Although this analysis established the general footprint of gelsolin on actin, the resolution of this reconstruction does not permit the orientation of gelsolin domain 2 with respect to the filament to be unambiguously determined.

The work presented here seeks to construct a preliminary atomic model of gelsolin domain 2 in complex with filamentous actin. We report the 1.75 Å crystal structure of domain 2 from severin, the gelsolin homologue from *Dictyostelium discoideum* (*17*). A structure-based alignment of severin domain 2 and other gelsolin family domains

[†] This work is supported by a research grant from the National Institutes of Health (Grant GM53807 to S.C.A.). Beamline X9B at the National Synchrotron Light Source is supported by Grant RR01633 from the Department of Energy. Y.A.P. is supported by an MSTP grant from the NIH (T32 GM07288).

[‡] The crystal structure of severin domain 2 has been deposited in the RCSB Protein Data Bank as file 1SVY.

* To whom correspondence should be addressed: Department of Biochemistry, Albert Einstein College of Medicine, 1300 Morris Park Ave., Bronx, NY 10461. E-mail: almo@aecom.yu.edu.

[§] Albert Einstein College of Medicine.

[||] Ludwigs-Maximilians Universität München.

10.1021/bi992364d CCC: $19.00
Published on Web 04/13/2000

Table 1: Data Collection and Phasing Statistics for Severin Domain 2

	native 1	$K_2[Pt(CN)_6]$	$K[Au(CN)_4]$	EMP	native 2
concentration of heavy-atom compound (mM)	−	1	1	1	−
soak time	−	2 months	6 days	1 day	−
data collection statistics					
wavelength (Å)	1.54	1.54	1.54	1.54	1.20
temperature (K)	298	298	298	298	140
all data (reflections with $I > 0\sigma_I$)					
no. of reflections	4238	2737	3354	6255	10235
resolution (Å)	90−2.40	90−2.75	90−2.60	90−2.50	20.0−1.75
completeness (%)	92.2	88.5	91.9	85.4	93.1
R_{merge} (%)[a]	6.1	5.0	3.4	3.2	3.5
highest-resolution shell					
no. of reflections	332	222	274	510	822
resolution (Å)	2.49−2.40	2.85−2.75	2.69−2.60	2.59−2.50	1.81−1.75
completeness (%)	78.5	74.7	79.4	68.9	77.1
R_{merge} (%)[a]	15.8	13.1	7.0	10.2	11.6
phasing statistics for 15−2.8 Å data					
no. of sites	−	3	2	2	−
R_{cullis}[b]	−	0.635	0.640	0.610	−
R_{kraut}[c]	−	0.069	0.105	0.137	−
anomalous	−	−	−	0.156	−
mean FOM[d]	−	0.290	0.294	0.305	−
anomalous	−	−	-	0.268	−
phasing power[e]	−	1.100	1.160	1.430	−

[a] $R_{merge} = \Sigma_{hkl}\Sigma_n|\langle I(hkl)\rangle - I_n(hkl)|/\Sigma_{hkl}\Sigma_n I_n(hkl)$, where $I_n(hkl)$ and $\langle I(hkl)\rangle$ are the nth and mean measurements of the intensity of reflection hkl. [b] $R_{cullis} = \Sigma_{hkl}(|F_{PH}| - |F_P|) - |F_H{}^{calc}||/\Sigma_{hkl}||F_{PH}| - |F_P||$ for centric reflections only, where F_{PH} and F_P are the structure factors for the native and derivative crystals, respectively, and $F_H{}^{calc}$ is the calculated structure factor based on the heavy-atom scattering. [c] $R_{kraut} = \Sigma_{hkl}||F_{PH}| - |\mathbf{F}_P + \mathbf{F}_H||/\Sigma_{hkl}|F_{PH}|$, where F_{PH} is the structure factor for the heavy-atom derivative and $\mathbf{F}_P$ and $\mathbf{F}_H$ are the calculated vectors for the contributions of the protein and heavy atoms, respectively, to the scattering. [d] FOM is the figure of merit, which equals $\langle|F_{best}(\phi^{calc})|/|F_P|\rangle$, which is the average ratio of the calculated protein structure factors, assuming a set of phases ϕ^{calc}, to the observed protein structure factors. [e] Phasing power $= \Sigma_{hkl}|F_H|/\Sigma_{hkl}||F_{PH}{}^{obs}| - |F_{PH}{}^{calc}||$.

implicated a number of domain 2 residues as contributing to a possible F-actin binding surface. The role of several of these residues in F-actin binding was tested by assaying mutants of gelsolin domain 2 for a decrease in filament-binding activity. The identification of an F-actin binding surface of gelsolin domain 2 has allowed for the construction of an atomic model of the gelsolin domain 1−domain 2−F-actin complex which is consistent with available biochemical and structural data. This model also suggests the existence of both positive and negative determinants for end-binding versus side-binding domains.

EXPERIMENTAL PROCEDURES

Purification and Crystallization of Severin Domain 2. Severin domain 2 was purified as described previously (*17*). The protein was dialyzed against 2 mM potassium phosphate (pH 6.8) and 2.8 mM β-mercaptoethanol, lyophilized, and stored at −20 °C. The lyophilized severin domain 2 was resuspended in 10 mM Tris-HCl (pH 8.0) and 1 mM DTT to yield a concentration of 20 mg/mL. Crystals took several months to grow at room temperature using the hanging drop vapor diffusion method, with 1.5 M sodium citrate and 100 mM HEPES (pH 8.0) as the precipitant.

Solution of the Crystal Structure of Severin Domain 2. One native data set (native 1, at 2.4 Å resolution) and three isomorphous derivatives were collected at room temperature on a Siemens X-1000 multiwire area detector coupled to a Rigaku RU-200 X-ray generator operating in fine focus mode at 55 kV and 85 mA (λ = 1.54 Å). All room-temperature data sets were reduced with XDS (*18*) and scaled with SCALEPACK (*19*) (Table 1).

An additional native data set (native 2, at 1.75 Å resolution) was collected with 1.20 Å radiation at beamline X9B at the National Synchrotron Light Source (Brookhaven National Laboratories, Upton, NY). The crystal was frozen in a stream of nitrogen vapor at 140 K, with mother liquor alone serving as the cryoprotectant. Data were collected in 2° frames on Fuji image plates, utilizing a custom-built apparatus as described previously (*20*). The synchrotron data set was reduced with DENZO and scaled with SCALEPACK (*19*) (Table 1).

Attempts at using the averaged or ensemble NMR structures of severin domain 2 (*21*) as a starting model for molecular replacement with either AMoRe (*22*) or X-PLOR (*23*) failed. Three heavy atom derivatives, $K_2[Pt(CN)_6]$, $K[Au(CN)_4]$, and ethylmercury phosphate (EMP), were used to solve the phase problem by multiple isomorphous replacement with anomalous scattering (MIRAS) (Table 1). The program VERIFY (S. L. Roderick, unpublished program) was used in conjunction with the PHASES-95 suite of programs (*24*) to locate the heavy atom sites for each derivative. Phases were calculated with PHASES-95 using 15−2.8 Å data from all three derivatives, including the anomalous scattering contribution from the EMP derivative (Table 1), resulting in a combined mean figure of merit of 0.579. The map was solvent-flattened using the program DM (*25*), resulting in a map of sufficient quality to allow the backbone chain to be traced (Figure 1).

Model building into the 2.8 Å map was performed with the program O (*26*) using the averaged NMR structure (*21*) as a guide. Initial refinement cycles consisted of 4000 K simulated annealing and positional and temperature factor refinement with X-PLOR 3.851 (*23*), using 8.0−2.4 Å data from the native 1 data set, with 10% of the reflections sequestered for calculation of R_{free} (*27*). Later refinement cycles were carried out against 20−1.75 Å data from the

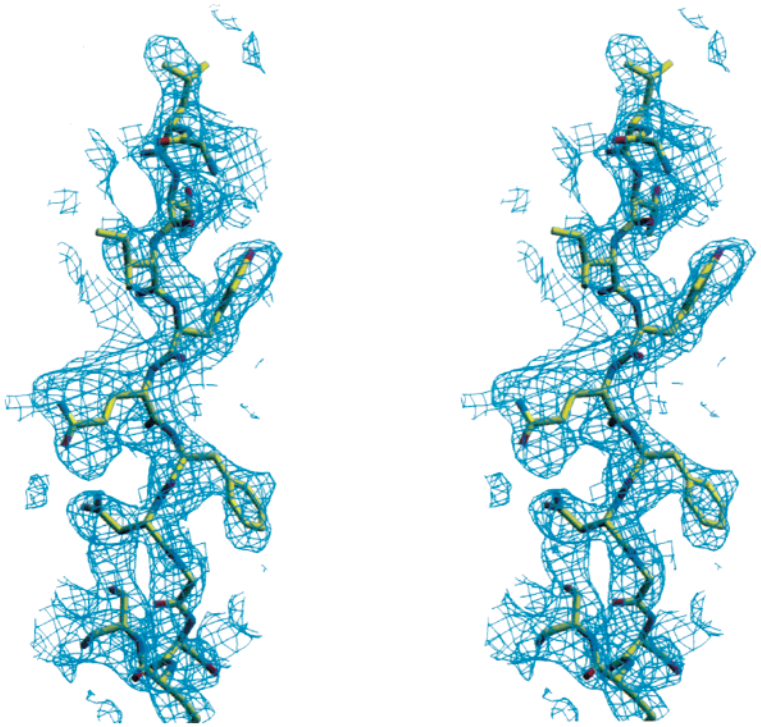

FIGURE 1: Stereoimage of the experimental electron density map of severin domain 2. The solvent-flattened MIRAS map is contoured at 0.9σ. Density is superimposed over the coordinates of the refined 1.75 Å structure. This figure was generated with SETOR (*52*).

high-resolution native 2 data set, and incorporated a bulk solvent model (*28*). On the basis of coordination geometry (*29*−*31*), temperature factors, and homology with the cation binding sites in gelsolin domain 1 (*8*), two water molecules were replaced with a sodium ion and a calcium ion (Figure 2a). Strong residual $F_o - F_c$ density near the sulfur atom of Cys235 suggested that the side chain had oxidized, so the amino acid was modeled as *S*-hydroxycysteine. Standard procedures were followed to ensure good model building throughout refinement (*32*), including simulated annealing OMIT maps and verification of stereochemical quality with PROCHECK (*33*) and WHAT IF (*34*).

Structure-Based Alignment of Gelsolin Domain 1 and 2 Homologues. Initially, the crystal structures of gelsolin domain 1 (*8*), gelsolin domain 2 (*35*), and severin domain 2 were superimposed using the structural alignment program DALI (*36*). This alignment was examined in O (*26*) and adjusted manually. CLUSTAL W (*37*) was implemented in aligning the sequences of domains without crystal structures (Figure 3). Superpositions and calculations of α-carbon rmsd values were performed using the program ProFit, version 1.6 (*38*). Surface areas were calculated using Richmond's modification (*39*) of the algorithm of Lee and Richards (*40*), as implemented in the program VADAR (*41*).

Subcloning and Mutagenesis of GST−*Gelsolin Domain 2.* The coding sequence for human gelsolin domain 2 (residues 151−266 of cytoplasmic gelsolin) (*42*) was ligated into the *Bam*HI and *Eco*RI sites of the GST fusion vector pGEX-4T-2 (Pharmacia). This construct, named pGEX/G2, resulted in the replacement of the N-terminal Met with the Gly-Ser segment after the thrombin cleavage site. Three mutations, RRV168AAA, RLK210AAA, and K218A, were created using the Stratagene Quik-Change protocol, and were confirmed by DNA sequencing.

Purification of Wild-Type and Mutant Gelsolin Domain 2. BL21(DE3) cells (Novagen) were transformed with wild-type or mutant gelsolin domain 2 constructs. Six liters of LB containing 100 mg/L ampicillin was inoculated with a 1:1000 dilution of an overnight culture and grown at 37 °C until an OD_{600} of 1.0 was reached. The cells were then induced with 1 mM IPTG for 3−5 h, after which the cells were harvested by centrifugation and the pellets stored at −20 °C.

The purification of wild-type and mutant gelsolin domain 2 proceeded essentially identically. Frozen cell pellets from 6 L of culture were resuspended in 90 mL of sucrose lysis buffer [50 mM Tris-HCl (pH 8.0), 25% sucrose, 1 mM EDTA, 0.1 mM DTT, and 0.1 mM NaN_3] with 9000 units of DNase I and 30 mg of chicken egg white lysozyme. The mixture was rocked on a Nutator at room temperature for 1 h followed by lysis by three passes through a French press operating at 1000 psi, and the crude lysate was centrifuged in a Sorvall SS-34 rotor at 18 000 rpm for 1 h at 4 °C. The pellet was resuspended in 75 mL of deoxycholate buffer [20 mM Tris-HCl (pH 8.0), 0.2 M NaCl, 2 mM EGTA, 1% sodium deoxycholate, 0.1 mM DTT, and 0.1 mM NaN_3] and centrifuged again at 18 000 rpm for 30 min. The resulting pellet was resuspended in 75 mL of distilled water and the mixture centrifuged again at 18 000 rpm for 30 min. The final pellet was dissolved in 75 mL of urea/PBS/DTT buffer (7 M urea, 140 mM NaCl, 2.7 mM KCl, 10 mM Na_2HPO_4, 1.8 mM KH_2PO_4, and 0.5 mM DTT) overnight at 4 °C. The supernatant was clarified by centrifugation at 18 000 rpm for 30 min, decanted, and brought to a final volume of 750 mL by the addition of urea/PBS/DTT buffer, and then dialyzed overnight against 16 L of PBS/DTT buffer (140 mM NaCl, 2.7 mM KCl, 10 mM Na_2HPO_4, 1.8 mM KH_2PO_4, and 0.5 mM DTT). The dialysate was clarified by

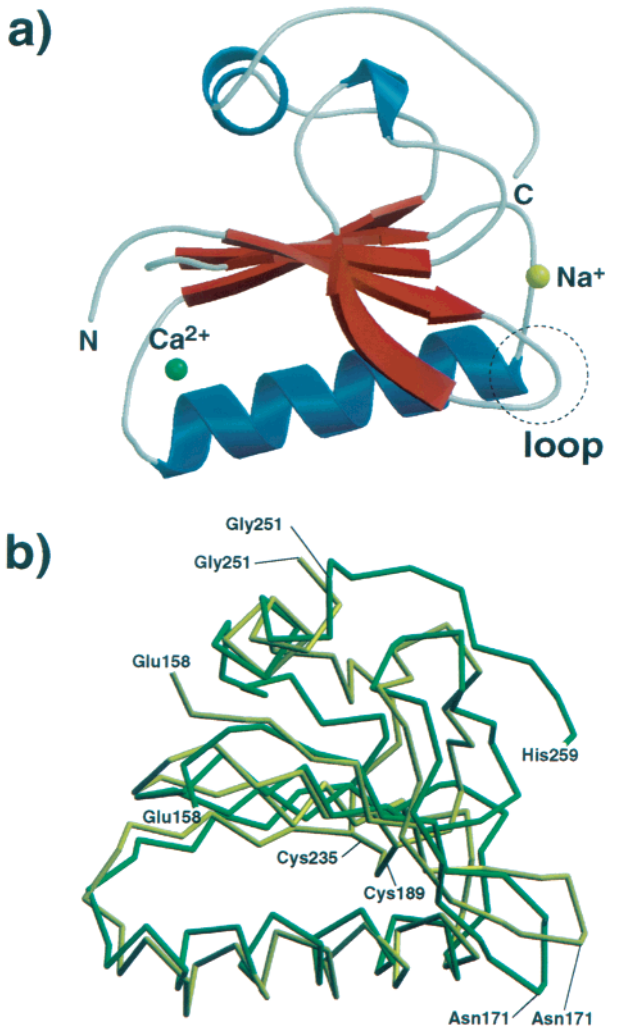

FIGURE 2: Overall structure of severin domain 2. (a) Ribbon diagram of the crystal structure of severin domain 2 with bound cations. This figure was generated with MOLSCRIPT (*53*) and Raster3D (*54*). The three-residue loop conserved in all gelsolin domain 2 homologues (severin domain 2 residues 169−171) is circled. (b) Comparison of crystal and NMR structures of severin domain 2. The α-carbon traces of the crystal structure (green) and the NMR structure (yellow) are shown superimposed. The Cys189−Cys235 disulfide bond is present only in the NMR structure. This figure was generated with SETOR (*52*).

filtration through a 0.65 μm DuraPore membrane filter (Millipore).

The protein was loaded onto a 20 mL glutathione Sepharose 4B column (Pharmacia), and the column was washed with 1 L of PBS/DTT and then with 100 mL of thrombin cleavage buffer [10 mM Tris-HCl (pH 8.0), 0.1 M NaCl, 2.5 mM $CaCl_2$, and 0.5 mM DTT]. The fusion protein was cleaved on the column with 250 μg of thrombin for 2 h at room temperature, followed by the addition of PMSF to a concentration of 1 mM. Gelsolin domain 2 was eluted from the column with 50 mL of thrombin cleavage buffer.

The eluate was concentrated to a volume of <10 mL and gel filtered on a 2.5 cm × 50 cm Sephacryl S-200 column equilibrated in F buffer [1.8 mM Tris-HCl (pH 8.0), 0.45 mM DTT, 0.18 mM $CaCl_2$, 0.9 mM NaN_3, 150 mM KCl, 2 mM $MgCl_2$, and 1 mM EGTA]. Fractions containing pure protein were pooled and concentrated. Following dialysis against F buffer, the protein was clarified by ultracentrifugation in a Beckman TL-100.2 rotor at 95 000 rpm for 30 min. The molecular weights of wild-type and mutant proteins were verified by ESI-MS (Table 3). Typical yields were approximately 2 mg of protein per liter of culture.

Urea Denaturation Assays. Fluorescence emission spectra were collected on a Photon Technology International fluorescence system (version 1.2x) with an excitation wavelength of 295 nm, an emission wavelength of 355 nm, an integration time of 2 s, and all slits set to a width of 2 nm. Samples consisted of 1 μM protein in 150 mM KCl, 2 mM Tris-HCl (pH 8.0), 0.5 mM DTT, 2 mM $CaCl_2$, and 0−8.5 M urea, maintained at 25.0 ± 0.1 °C. All buffers were passed through a 0.22 μM filter before use. All urea denaturation curves were normalized and fit using KaleidaGraph version 3.0 (Synergy Software) to a linear extrapolation model relating a sigmoidal denaturation curve to the Δ*G* of unfolding (*43*).

F-Actin Cosedimentation Assays. Rabbit skeletal muscle actin was prepared from acetone powder by a modification of the method of Spudich and Watt (*44*), followed by gel filtration on a 2.5 cm × 50 cm Sephacryl S-200 column. The samples for the cosedimentation assay consisted of 7.8 mM Tris-HCl (pH 8.0), 0.45 mM DTT, 2.0 mM $CaCl_2$, 0.9 mM NaN_3, 150 mM KCl, 2 mM $MgCl_2$, 1 mM EGTA, 0.2 mM Na_2ATP, and 15 μM actin-binding protein, with the concentration of F-actin varying from 0.5 to 90 μM. Samples without actin served as controls to ensure that wild-type and mutant gelsolin domain 2 alone did not sediment appreciably. Horse skeletal muscle myoglobin at a concentration of 15 μM was used as a negative control. The samples were incubated at 37 °C for 2 h, and then centrifuged at room temperature in a Beckman Airfuge at 25 psi (~130000*g*) for 30 min. Samples of the mixture, supernatant, and pellet were analyzed on 12% SDS−PAGE tricine gels. The gels were scanned on a Molecular Dynamics Computing Densitometer, and the intensities of the bands were quantified using the program ImageQuant 5.0.

The concentration of gelsolin domain 2 in the pellet, $[G2]_{bound}$, was plotted against the concentration of F-actin in the pellet, $[A]_{pel}$, to generate a binding isotherm, which was fit to the equation

$$[G2]_{bound} = 0.5[([actin]_{pel} + [G2]_{total} + K_d) - [([actin]_{pel} + [G2]_{total} + K_d)^2 - 4[actin]_{pel}[G2]_{total}]^{1/2}]$$

which takes into account ligand depletion (*45*). The binding constant K_d was estimated by a nonlinear least-squares fit using the program KaleidaGraph.

Construction of a Model of the Gelsolin Domain 2−F-Actin Complex. Gelsolin domain 1 was first docked onto the side of the Lorenz model of F-actin (*46*) with the binding mode observed in the gelsolin domain 1−G-actin complex (*8*). Gelsolin domain 2 was then superimposed onto domain 1 on the basis of the structural alignment. Superpositions were performed with the program ProFit (*38*).

RESULTS

Quality of the Severin Domain 2 Crystal Structure. The structure of severin domain 2 was determined with three heavy atom derivatives (Table 1) that yielded an interpretable 2.8 Å map (Figure 1). The NMR structure was manually docked into the experimental density; the model was rebuilt

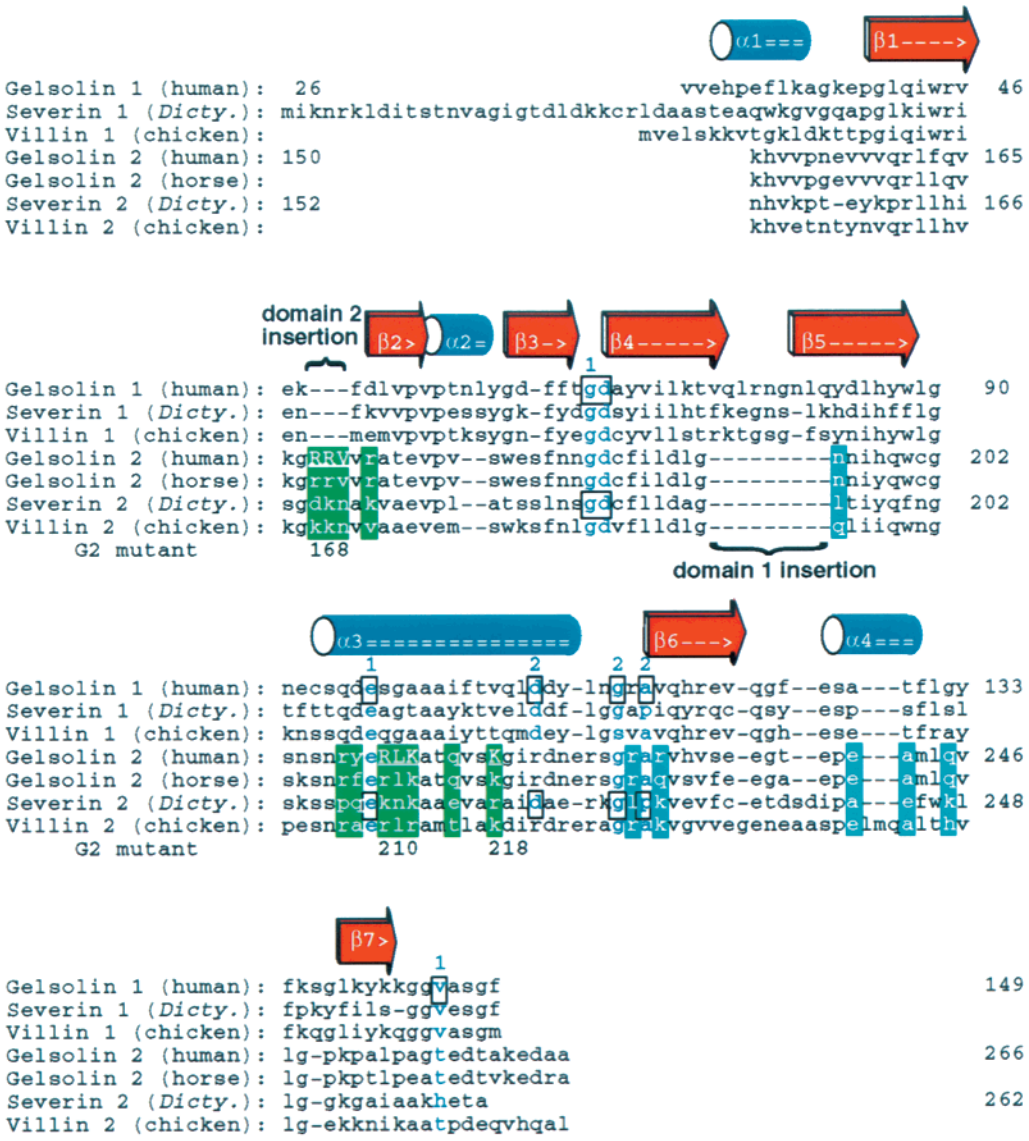

FIGURE 3: Structure-based alignment of end-binding and side-binding gelsolin domains. Insertions specific to end-binding or side-binding domains are noted. Residues predicted to be involved in binding F-actin in a domain 1-like mode are indicated by the green boxes. Gelsolin domain 2 residues mutated in this study are capitalized and underlined, with the residue numbers shown in the row labeled "G2 mutant". Residues predicted to compose another surface involved in contacting a second actin molecule in the context of F-actin are indicated by the cyan boxes. Black outlines indicate residues crystallographically observed to interact directly with a bound cation corresponding to the intramolecular site in gelsolin 1 (indicated by the blue label 1) or the intermolecular site (labeled 2). Blue residues are residues predicted but not yet observed to bind cations. The secondary structural elements shown are derived from the structure of gelsolin domain 1.

and refined to 2.4 Å resolution, and the resolution was subsequently extended to 1.75 Å. The final model contains residues 158−259 (out of 152−262), 114 ordered water molecules, and two bound cations (Table 2).

The model possesses good geometry, with an rms deviation from ideal bond lengths of 0.008 Å and an rms deviation from ideal bond angles of 1.36°; 98.8% of all non-glycine, non-proline residues were in the most favored and additionally allowed regions of the Ramachandran plot (Table 2). One residue, Asp169, is in a disallowed region close to the border of a generously allowed region; this minor stereochemical violation is likely due to a local distortion induced by the participation of Asp169 in a cation-binding site.

Comparison with Other Gelsolin Family Domains. Severin domain 2 displays the same architecture observed in other gelsolin family domains, a mixed parallel/antiparallel five-stranded β-sheet, flanked on one side by a long α-helix running parallel to the sheet and flanked on the other by a shorter α-helix running perpendicular to the sheet (Figure 2a). A superposition (*38*) of the crystal structure of severin domain 2 with the minimized average NMR structure (*21*) yielded a surprisingly large α-carbon rmsd of 2.5 Å (Figure 2b); for comparison, the α-carbon rms deviations of the crystal structure of severin domain 2 superimposed on gelsolin domain 1 or gelsolin domain 2 are 1.7 and 2.7 Å, respectively. The most notable difference is a nonphysiological disulfide bond present in the NMR structure of severin domain 2 (Figure 2b), which results in large conformational differences between the crystal and NMR structures in the vicinity of Cys189 and Cys235. Additional differences between the structures are seen in linker regions which were not well ordered in the original NMR structure (residues 168−173, 193−197, 225−229, and 233−243). Despite these local differences between the NMR and crystal

Table 2: Refinement Statistics for the Native 2 Data Set

space group	$P2_12_12_1$
unit cell parameters	$a = 33.35$ Å, $b = 49.22$ Å, $c = 62.79$ Å, $\alpha = \beta = \gamma = 90°$
all data ($I/\sigma_I > 0.0$)	
resolution (Å)	20−1.75
R_{cryst}[a]	0.184
R_{free}[b]	0.246
highest-resolution shell	
resolution (Å)	1.83−1.75
R_{cryst}[a]	0.274
R_{free}[b]	0.320
rms deviations from ideality[c]	
bond lengths (Å)	0.008
bond angles (deg)	1.36
Ramachandran plot statistics[d]	
most favored regions	90.8% (79)
additional allowed regions	8.0% (7)
generously allowed regions	0.0% (0)
disallowed regions	1.1% (1)
residue range	158−259
no. of atoms	
protein	773
water	114
Ca^{2+}	1
Na^{+}	1
all atoms	889
average B factor (Å^2)	
protein atoms	18.2
waters	33.1
Ca^{2+}	32.3
Na^{+}	23.8
all atoms	20.1

[a] $R_{cryst} = \Sigma_{hkl}|F_o - F_c|/\Sigma_{hkl}F_o$, where F_o and F_c are the observed and calculated structure factor amplitudes, respectively, for all reflections hkl used in refinement (90% of the data). [b] R_{free} is R_{cryst} calculated for 10% of the data which were sequestered and not used in refinement (*27*). [c] As calculated by WHAT IF (*34*) using the stereochemical criteria of Engh and Huber (*51*). [d] As determined for all non-glycine, non-proline residues by PROCHECK (*33*).

Table 3: Mutant and Wild-Type Human Gelsolin Domain 2

sequence	predicted MW[a]	ESI-MS MW[a]	$\Delta G_{folding}$ (kcal/mol)	fraction folded[b]	K_d for F-actin (mM)
wild-type	13 010.5	13 009.0	7.1	0.999994	7.9 ± 0.6
RRV168AAA	12 812.2	12 810.0	5.6	0.99992	36.3 ± 4.3
RLK210AAA	12 826.2	12 825.0	3.1	0.9974	329 ± 19
K218A	12 953.4	12 951.0	3.9	0.99995	9.4 ± 1.5

[a] Includes the N-terminal Gly-Ser fragment from the thrombin cleavage site. [b] As calculated from the ΔG by the Boltzmann distribution.

structures, the overall position and orientation of the secondary structural elements are essentially the same.

Cation-Binding Sites in Severin Domain 2. In the course of refinement, two features likely to be bound cations were identified: a sodium ion, which originated from the 1.5 M sodium citrate precipitant, and a calcium ion, presumably residual from the purification. The putative sodium ion is coordinated by the carbonyl oxygen Gly187 O, Oδ1 from Asp188, both Oϵ1 and Oϵ2 from Glu210, and water molecule W32. Water W32 is within hydrogen-bonding distance of Gly187 O, Lys205 O, Ser207 N, and Asp169 Oδ1 (which may account for the suboptimal stereochemistry of Asp169). The putative calcium ion is coordinated by Asp222 Oδ1 and Oδ2, Gly227 O, Pro227 O, and three water molecules (W13, W22, and W37).

Identification of a Potential F-Actin Binding Surface. To identify residues which may be part of the F-actin binding surface of gelsolin domain 2, we constructed a structure-based alignment of the end-binding domain 1 homologues and the side-binding domain 2 homologues (Figure 3). The alignment revealed significant differences between end-binding and side-binding domains: (1) a three-residue basic insertion between β-strands 1 and 2 (gelsolin domain 2 residues 168−170) unique to the side-binding domains, (2) the presence of conserved basic residues on the long helix of the side-binding domains (typically small aliphatic residues in end-binding domains), and (3) an eight- or nine-residue insertion between β-strands 4 and 5 (gelsolin 1 residues 74−82) unique to the end-binding domains (Figures 3 and 4a).

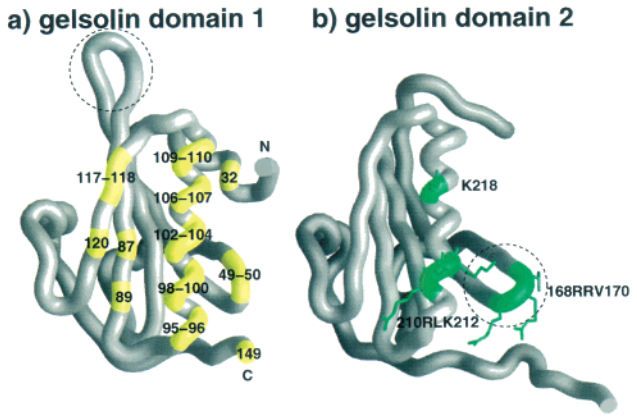

FIGURE 4: Comparison of end-binding and side-binding surfaces. (a) Backbone worm of gelsolin domain 1, with residues involved in binding G-actin (*8*) labeled. The eight-residue loop specific to domain 1 homologues is circled. (b) Backbone worm of gelsolin domain 2 (*35*), with residues mutated in this work labeled. The three-residue loop specific to domain 2 homologues is circled. This figure was generated with GRASP (*55*).

The first two surface features, the $\beta1-\beta2$ loop and the basic surface of the long helix, are present only in side-binding domains and absent in end-binding domains, and are on the same face of gelsolin domain 2, consistent with the idea that they contribute to a continuous side-binding surface (Figure 4b). This putative side-binding face of gelsolin domain 2 corresponds topologically to the end-binding surface of gelsolin 1 (Figure 4a). To test whether these features do, in fact, constitute an F-actin binding surface, three mutants of human gelsolin domain 2 were constructed, one mutant probing the role of the $\beta1-\beta2$ loop by mutating 168RRV170 to AAA, and two mutants testing the importance of the long helix by changing 210RLK212 to AAA and K218 to A (Figures 3 and 4b).

Verification of Wild-Type and Mutant Gelsolin Domain 2 Stability. Urea denaturation studies were carried out to ensure that the wild-type and mutant proteins were stable and folded. Curves obtained from all four proteins in the presence of calcium (Figure 5) displayed a sigmoidal shape, consistent with a single-domain protein unfolding cooperatively in a simple, two-state process (*43*). The approximate ΔG values for the folded → unfolded transition derived from these curves indicate that wild-type and mutant proteins are all at least 99.7% folded (Table 3).

F-Actin Binding Activity of Wild-Type and Mutant Gelsolin Domain 2. The affinities of wild-type and mutant gelsolin domain 2 constructs for actin filaments were measured with an F-actin cosedimentation assay. Wild-type gelsolin domain 2 bound F-actin with a K_d of 7.9 μM in the presence of

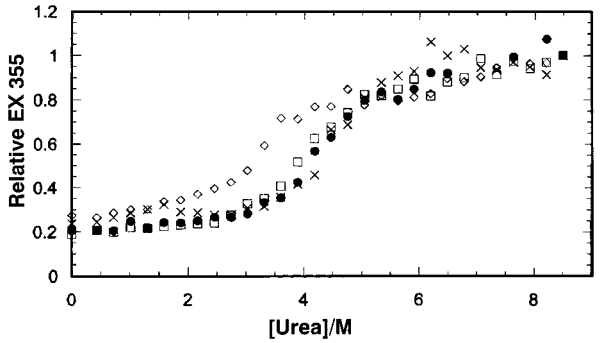

FIGURE 5: Urea denaturation curves of wild-type and mutant gelsolin domain 2. The black circles (●) represent measurements for wild-type gelsolin domain 2, the boxes (□) those for the RRV168AAA mutant, the diamonds (◇) those for RLK210AAA, and the crosses (×) those for K218A.

calcium (Table 3 and Figure 6a), which is consistent with the values of 7.1 μM (*42*) and 1.4 μM (*14*) reported previously. The K_d values measured for mutants RRV168AAA, RLK210AAA, and K218A were 36.3, 329, and 9.4 μM, respectively (Table 3 and Figure 6b−d). The RRV168AAA mutant binds with 4−5-fold lower affinity than the wild type; the RLK210AAA mutant has little or no affinity for F-actin, and the affinity of the K218A mutant for actin filaments is indistinguishable from that of the wild type.

Model of the Gelsolin Domain 1−Domain 2−F-Actin Complex. The gelsolin domain 1−domain 2−F-actin model depicted in Figure 7 utilizes the domain 1−G-actin structure of McLaughlin and co-workers (*8*) to represent the end-binding interaction, and assumes a "domain 1-like" binding mode for gelsolin domain 2. Since this model results in some interpenetration of gelsolin 2 and the filament, local rearrangements must occur to prevent unfavorable steric interactions. However, the notion of a "domain 1-like" binding mode serves as a useful heuristic in predicting which residues in gelsolin domain 2 may interact with the side of the actin filament.

In this gelsolin domain 2−F-actin model (Figure 7), the predicted side-binding residues (green boxes in Figure 3) are part of a domain 1-like binding surface (green residues in Figure 8a). In addition, several residues on the short α-helix (Glu241, Ala242, and Gln245) and on the edge of the β-sheet (Asn195, Arg228, Arg230) are predicted to contribute to a second side-binding surface (Figure 8b) on the basis of their proximity to a second actin monomer in the filament (Figure 7), their large accessible surface area (data not shown), and their conservation among other domain 2 homologues (Figure 3).

DISCUSSION

High-Resolution Structure of an F-Actin Binding Gelsolin Domain. The structure of severin domain 2 is the first crystal structure of a nonmammalian gelsolin family domain. Severin domain 2 exhibits the canonical gelsolin domain fold, and allows for an extensive structure-based alignment that highlights structural features specific to the side-binding and end-binding domains. Side-binding domains are distinguished by the presence of the three-residue basic insertion between β-strands 1 and 2 (gelsolin domain 2 residues 169−171), the absence of the long loop between β-strands 4 and 5 observed in end-binding domains (gelsolin 1 residues 74−82), and conserved basic residues on the surface of the long α-helix (gelsolin domain 2 residues 207−223).

Two cations were found in the crystal structure of severin domain 2, located at each end of the long α-helix (Figure 2a), at sites which correspond closely to calcium-binding sites suggested by NMR titration studies (*21*). These sites can also

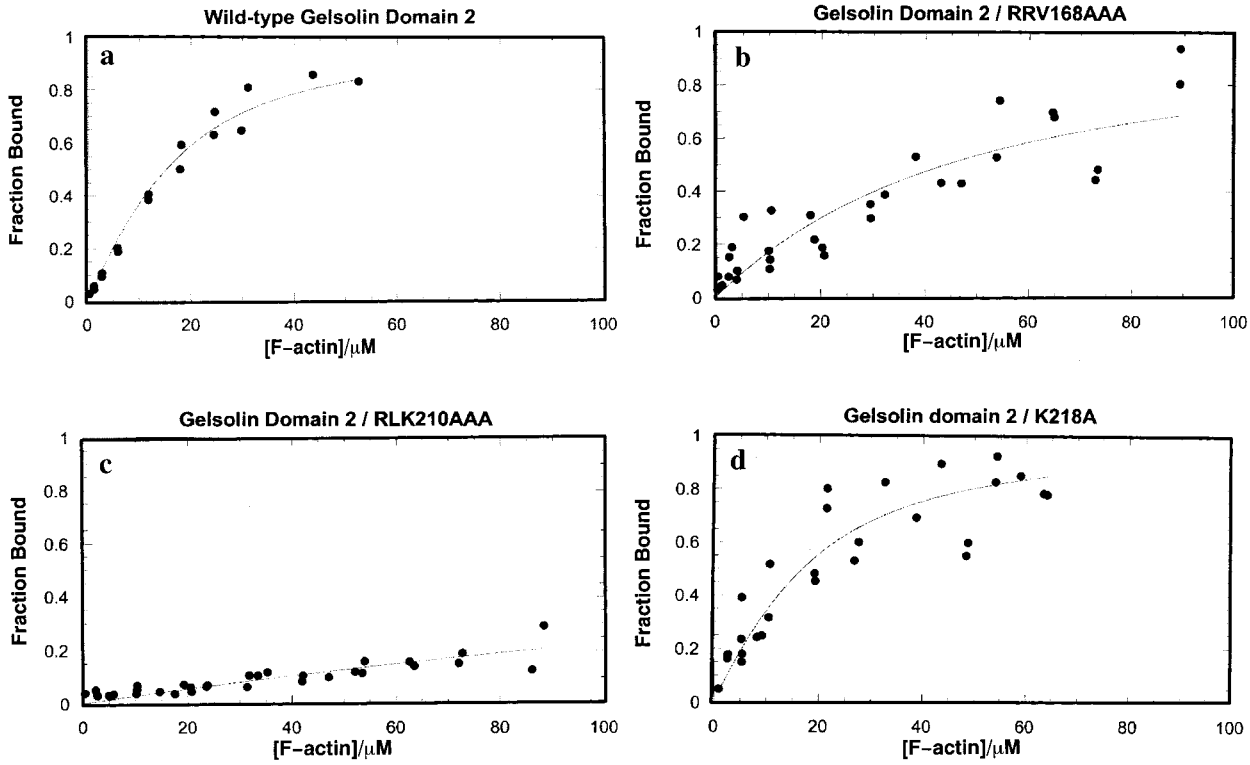

FIGURE 6: F-Actin binding curves of wild-type (a) and mutant (b−d) gelsolin domain 2.

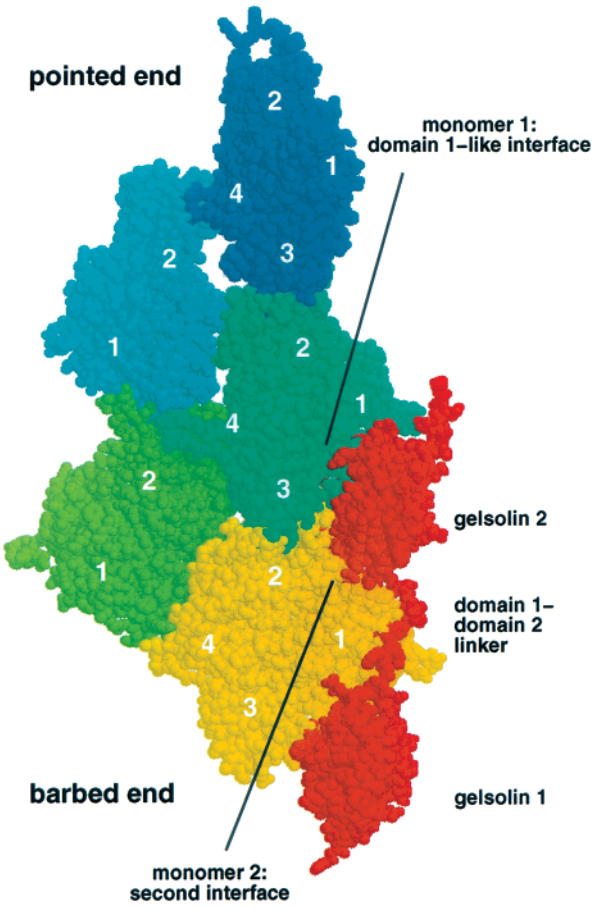

FIGURE 7: Model of the complex of F-actin and gelsolin domains 1 and 2. The monomer subdomains and the ends of the filament are labeled. The domain 1−barbed end interaction is modeled by the domain 1−G-actin structure of McLaughlin and co-workers (*8*). The interaction of domain 2 with F-actin is modeled using a domain 1-like interaction. The two sites of contact between gelsolin domain 2 and the filament in this model are indicated. This figure was generated with GRASP (*55*).

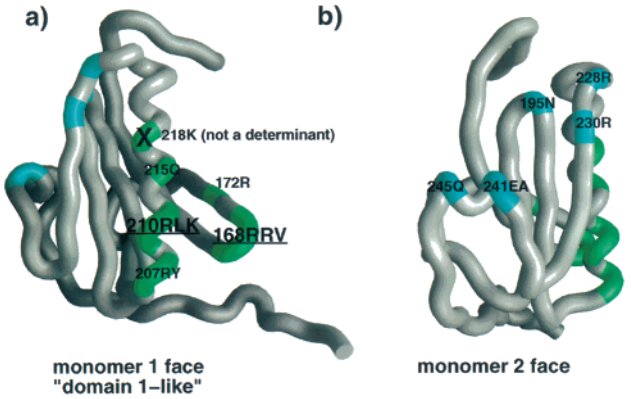

FIGURE 8: Prediction of gelsolin domain 2 residues involved in F-actin binding. Residues involved in the domain 1-like binding mode are indicated in green; underlined labels indicate residues experimentally determined in this work to be involved in binding F-actin. Residues on a face of gelsolin domain 2 which may contact a second monomer with the actin filament are indicated in cyan. The two views are rotated by approximately 90°. This figure was generated with GRASP (*55*).

be superimposed on the corresponding calcium-binding sites in gelsolin domain 1 (*8*) and villin domain 1 (*47*, *48*). The direct observation of cations bound to both end-binding and side-binding domains at analogous sites suggests a conservation of sites over the course of the evolution of gelsolin family domains.

The overall structure of severin domain 2 is similar to the NMR structure, although there are a number of local differences which can be attributed to crystal packing, the disulfide bond in the NMR structure, and the differences inherent in structures determined by NMR versus crystallography (*49*). The greater precision and accuracy of side chain positions in the crystal structure and the closer correspondence to other gelsolin domains make the crystal structure a preferable choice for structural comparisons.

F-Actin Binding Surface of Gelsolin Domain 2. From a structure-based alignment and mutagenesis studies, a filament-binding surface of gelsolin domain 2 has been identified. This side-binding surface is topologically similar to the end-binding surface of gelsolin domain 1 (Figure 4), and consists primarily of basic residues, as would be predicted to interact with the acidic surface of filamentous actin. Two features of gelsolin domain 2 whose roles in binding F-actin have been experimentally verified are the conserved loop between β-strands 1 and 2, as demonstrated by the RRV168AAA mutant, and the long α-helix, as shown by the RLK210AAA mutant (Figures 3 and 4b).

These mutagenesis results are essentially in agreement with all prior peptide, deletion, and mutagenesis studies. The role of the three-residue loop of gelsolin residues 168−170 is consistent with studies which demonstrated side-binding activity for a villin domain 2 peptide consisting of residues 132−147, corresponding to gelsolin residues 159−171 (*13*). In the same study, mutants of some of these same residues in intact villin domains 1−3, namely, R137A, K142A, K144A, K145A (which correspond to gelsolin residues 161, 166, 168, and 169), were found to have significantly decreased severing activities; however, the study presented here suggests that the villin K144A and K145A mutations may have altered severing activity merely by decreasing the affinity of villin for filamentous actin. A deletion of gelsolin domain 2 residues 150−172 (*14*), which also encompasses this loop, abolished side-binding activity in gelsolin domain 2, but it is more likely that the deletion unfolds the protein by disrupting the central β-sheet (*35*). The significant role of the long helix (residues 207−223) in binding to F-actin is corroborated by a study in which a peptide spanning gelsolin domain 2 residues 198−227 (which contains the long helix, and residues 210RLK212) possesses weak filament-binding activity, with a K_d of 125 μM (*11*).

A Model of the Gelsolin Domain 1−Domain 2−F-Actin Complex. The mutagenesis studies presented here are consistent with prior biochemical studies in identifying residues on one surface of gelsolin domain 2 as part of the side-binding surface (Figure 4b). Since this surface bears a striking similarity to the end-binding surface of gelsolin domain 1 (Figure 4a), a model was constructed where gelsolin domain 2 was docked to the side of the filament in a domain 1-like binding mode. This model of gelsolin domain 2 bound to the filament is consistent with a number of biochemical and structural findings. In the domain 1-like binding mode depicted in Figure 7, the domain 2 loop of residues 168−170 is in the general vicinity of actin residues 1−5, 21−28, and 345−351 in the upper monomer, and domain 2 helix residues 210−212 may contact actin residues 144−146 and 335−349. The depicted binding mode of gelsolin domain 2

also has its N-terminus oriented toward the barbed end of the filament. When gelsolin 1 is docked onto the end of the filament, there is a distance of approximately 31 Å between the α-carbon of gelsolin 1 residue 149 and the α-carbon of gelsolin domain 2 residue 160, a distance which can be spanned by the 10 intervening residues (Figure 7). The model of the gelsolin domain 2−F-actin complex also compares favorably with the binding mode proposed by McGough et al. (*16*) on the basis of cryoelectron microscopy studies, since in both models, contacts with the upper monomer involve subdomains 1 and 3, most notably, actin residues 23, 146, and 350 (compare to Figure 6 of ref *16*).

The proposed binding mode delineates *two* filament-binding surfaces on gelsolin domain 2: one of these is the domain 1-like binding surface which was predicted and experimentally tested in this work (Figure 8a), and the second is a new binding surface, not previously identified, which interacts with the lower monomer. This second surface is on a different face of gelsolin domain 2, approximately 90° away from the domain 1-like binding surface (Figure 8b). Once the relevant residues were identified on the basis of proximity to the second monomer, it was found that they were conserved and frequently basic (cyan boxes in Figure 3). This is the first indication of a functional role for the short helix in any gelsolin family domain.

The second surface of gelsolin domain 2 appears to interact with subdomains 1 and 2 of the lower monomer in the actin filament, possibly mediated by actin residues 38−62 (which encompass the mobile DNase I binding loop) and 92−95. Despite the fact that the model was constructed in the absence of any constraints on the relative positions of gelsolin domain 2 and the lower monomer, the resulting interface with the lower monomer agrees favorably with that identified by McGough et al., which includes actin residues 46, 61, and 92 (see Figure 6 of ref *16*).

The model agrees favorably with biochemical studies attempting to determine the surface of F-actin covered by gelsolin. Feinberg et al. (*50*) showed that gelsolin domain 2 prevented the binding of antibodies directed against actin residues 1−10 and 18−28, which are approached by gelsolin residues 168−170 (the loop) and 240−247 (the short helix) in this model. The model is also consistent with the results of Van Troys and co-workers (*11*), who showed that antibodies against actin residues 12−44, 228−257, or 354−375 were not blocked by gelsolin domains 2 and 3.

Positive and Negative Determinants of End Binding and Side Binding. Biochemical and structural work on gelsolin domains 1 and 2 has typically focused on positive determinants of ligand binding. However, negative determinants must also exist, as there is no cross-reactivity between end-binding and side-binding domains. McLaughlin and co-workers (*8*) docked gelsolin 1 to the side of the Lorenz model of F-actin and noted that it could not bind the filament with its normal monomer-binding mode due to steric clashes; our modeling studies indicate that the bulk of the unfavorable contacts are due to the gelsolin 1 loop containing residues 73−82. This loop is present only in end-binding domains, where it is a ubiquitous feature, even though it has no role in binding monomeric actin (Figures 3 and 4a). Thus, the insertion may be a necessary negative determinant for preventing the binding of domain 1 to the side of actin filaments.

Gelsolin domain 2 also appears to possess negative determinants which prevent G-actin binding. Residues 168RRV170, R207, 211LK212, 214TQ215, and R221 are all predicted to prevent gelsolin domain 2 from binding to monomeric actin by steric interference (not shown). Many of these residues correspond to the positive determinants of F-actin binding determined by our mutagenesis studies, including the loop of residues 168−170 and the basic residues in the long α-helix (Figure 4b).

Conclusions. In the study presented here, the crystal structure of severin domain 2 was determined and refined to 1.75 Å resolution, and this structure was used in comparisons with other gelsolin family domains to predict a possible side-binding surface on gelsolin domain 2. By mutagenesis, it has been shown that human gelsolin domain 2 residues 168RRV170 and 210RLK212 are likely to be involved in filament binding, and K218 is probably not a determinant of F-actin binding. The experimental results were used to construct a model of the gelsolin domain 2−F-actin complex that is consistent with prior biochemical and structural studies. This model has identified other residues which may be involved in a second face that contacts the actin filament, and has also suggested the existence of negative determinants whose purpose is to prevent cross-reactivity of side- and end-binding domains.

ACKNOWLEDGMENT

The coding sequence for gelsolin domain 2 subcloned into vector pMW172 was a generous gift of Dr. Michael Way (EMBL, Heidelberg, FRG). Assistance with data collection at beamline X9B at Brookhaven National Laboratories was kindly provided by Mr. Michael Sullivan. We thank Dr. Gang Liu, Dr. Anne Bresnick, and Dr. John Condeelis for helpful advice on actin biochemistry and the cosedimentation assay, Dr. Anne Bresnick for many valuable comments on the manuscript, and Dr. Nicole Mahoney and Dr. Sergey Vorobiev for helpful discussions and advice.

REFERENCES

1. Matsudaira, P., and Janmey, P. (1988) *Cell 54*, 139.
2. Weeds, A., and Maciver, S. (1993) *Curr. Opin. Cell Biol. 5*, 63.
3. Puius, Y. A., Mahoney, N. M., and Almo, S. C. (1998) *Curr. Opin. Cell Biol. 10*, 23.
4. Janmey, P. A., Stossel, T. P., and Allen, P. G. (1998) *Chem. Biol. 5*, R81−R85.
5. Liu, Y. T., Rozelle, A. L., and Yin, H. L. (1998) in *G Proteins, Cytoskeleton, and Cancer* (Maruta, H., and Kohama, K., Eds.) pp 19−33, R. G. Landes Co., Austin, TX.
6. Kuzumaki, N., Fujita, H., Tanaka, M., Sakai, N., and Ohtsu, M. (1998) in *G Proteins, Cytoskeleton, and Cancer* (Maruta, H., and Kohama, K., Eds.) pp 121−132, R. G. Landes Co., Austin, TX.
7. Kwiatkowski, D. J. (1999) *Curr. Opin. Cell Biol. 11*, 103.
8. McLaughlin, P. J., Gooch, J. T., Mannherz, H. G., and Weeds, A. G. (1993) *Nature 364*, 685.
9. McGough, A., and Way, M. (1995) *J. Struct. Biol. 115*, 144.
10. Way, M., and Matsudaira, P. (1993) *Curr. Biol. 3*, 887.
11. Van Troys, M., Dewitte, D., Goethals, M., Vandekerckhove, J., and Ampe, C. (1996) *FEBS Lett. 397*, 191.
12. Van Troys, M., Dewitte, D., Verschelde, J. L., Goethals, M., Vandekerckhove, J., and Ampe, C. (1997) *J. Biol. Chem. 272*, 32750.
13. de Arruda, M. V., Bazari, H., Wallek, M., and Matsudaira, P. (1992) *J. Biol. Chem. 267*, 13079.

14. Sun, H. Q., Wooten, D. C., Janmey, P. A., and Yin, H. L. (1994) *J. Biol. Chem. 269*, 9473.
15. Tang, J. X., and Janmey, P. A. (1996) *J. Biol. Chem. 271*, 8556.
16. McGough, A., Chiu, W., and Way, M. (1998) *Biophys. J. 74*, 764.
17. Eichinger, L., and Schleicher, M. (1992) *Biochemistry 31*, 4779.
18. Kabsch, W. (1988) *J. Appl. Crystallogr. 21*, 916−924.
19. Otwinowski, Z., and Minor, W. (1997) *Methods Enzymol. 276*, 307.
20. Puius, Y. A., Zhao, Y., Sullivan, M., Lawrence, D. S., Almo, S. C., and Zhang, Z. Y. (1997) *Proc. Natl. Acad. Sci. U.S.A. 94*, 13420.
21. Schnuchel, A., Wiltscheck, R., Eichinger, L., Schleicher, M., and Holak, T. A. (1995) *J. Mol. Biol. 247*, 21.
22. Navaza, J., and Saludjian, P. (1997) *Methods Enzymol. 276*, 581.
23. Brünger, A. T. (1992) *X-PLOR Version 3.1: a System for Protein Crystallography and NMR*, Yale University Press, New Haven, CT.
24. Furey, W., and Swaminathan, S. (1997) *Methods Enzymol. 277*, 590.
25. Cowtan, K. D., and Main, P. (1991) *Acta Crystallogr., Sect. D 52*, 43.
26. Jones, T. A., Zou, J. Y., Cowan, S. W., and Kjeldgaard, M. (1991) *Acta Crystallogr., Sect. A 47*, 110.
27. Brünger, A. T. (1997) *Methods Enzymol. 277*, 366.
28. Jiang, J. S., and Brünger, A. T. (1994) *J. Mol. Biol. 243*, 100.
29. Nayal, M., and Di Cera, E. (1996) *J. Mol. Biol. 256*, 228.
30. Glusker, J. P. (1991) *Adv. Protein Chem. 42*, 1.
31. Brown, I. D., and Wu, K. K. (1976) *Acta Crystallogr., Sect. B 32*, 1957.
32. Kleywegt, G., and Jones, T. A. (1997) *Methods Enzymol. 277*, 208.
33. Laskowski, R. A., MacArthur, M. W., Moss, D. S., and Thornton, J. M. (1993) *J. Appl. Crystallogr. 26*, 283.
34. Vriend, G. (1990) *J. Mol. Graphics 8*, 52.
35. Burtnick, L. D., Koepf, E. K., Grimes, J., Jones, E. Y., Stuart, D. I., McLaughlin, P. J., and Robinson, R. C. (1997) *Cell 90*, 661.
36. Holm, L., and Sander, C. (1995) *Trends Biochem. Sci. 20*, 478.
37. Thompson, J. D., Higgins, D. G., and Gibson, T. J. (1994) *Nucleic Acids Res. 22*, 4673.
38. Martin, A. C. R. (1995) *ProFit V1.6: Protein Least Squares Fitting*, SciTech Software, Ashtead, Surrey, U.K.
39. Richmond, T. J. (1984) *J. Mol. Biol. 178*, 63.
40. Lee, B., and Richards, F. M. (1971) *J. Mol. Biol. 55*, 379.
41. Wishart, D. S., Willard, L., Richards, F. M., and Sykes, B. D. (1993) *VADAR V1.2: A Comprehensive Program Suite for Protein Structural Analysis*, University of Alberta, Edmonton, AB.
42. Way, M., Pope, B., and Weeds, A. G. (1992) *J. Cell Biol. 119*, 835.
43. Pace, C. N., and Scholtz, J. M. (1997) in *Protein Structure. A Practical Approach* (Creighton, T. E., Ed.) Chapter 12, IRL Press at Oxford University Press, New York.
44. Spudich, J. A., and Watt, S. (1971) *J. Biol. Chem. 246*, 4866.
45. Hulme, E. C., and Birdsall, N. J. M. (1992) in *Receptor-Ligand Interactions: A Practical Approach* (Hulme, E. C., Ed.) Chapter 4, IRL Press at Oxford University Press, New York.
46. Lorenz, M., Popp, D., and Holmes, K. C. (1993) *J. Mol. Biol. 234*, 826.
47. Markus, M. A., Nakayama, T., Matsudaira, P., and Wagner, G. (1994) *Protein Sci. 3*, 70.
48. Markus, M. A., Matsudaira, P., and Wagner, G. (1997) *Protein Sci. 6*, 1197.
49. Wagner, G., Hyberts, S. G., and Havel, T. F. (1992) *Annu. Rev. Biophys. Biomol. Struct. 21*, 167.
50. Feinberg, J., Benyamin, Y., and Roustan, C. (1995) *Biochem. Biophys. Res. Commun. 209*, 426.
51. Engh, R. A., and Huber, R. (1991) *Acta Crystallogr., Sect. A 47*, 392.
52. Evans, S. V. (1993) *J. Mol. Graphics 11*, 134.
53. Kraulis, P. J. (1991) *J. Appl. Crystallogr.*, 946.
54. Merritt, E. A., and Bacon, D. J. (1997) *Methods Enzymol. 277*, 505.
55. Nicholls, A., Bharadwaj, R., and Honig, B. (1993) *Biophys. J. 64*, 166.

BI992364D